The formation of a nanohybrid shish-kebab (NHSK) structure in melt-processed composites of poly (ethylene terephthalate) (PET) and multi-walled carbon nanotubes (MWCNTs)

Ellen L. Heeley[1]*, Darren J. Hughes[2], Eleanor M. Crabb[1], James Bowen[1], Oier Bikondoa[3], Beatriz Mayoral[4], Sandy Leung[5] and Tony McNally[5]

[1] Faculty of Science, Technology, Engineering and Mathematics, Open University, Walton Hall, Milton Keynes, MK7 6AA.
[2] WMG, University of Warwick, Coventry, CV4 7AL, UK.
[3] XMaS, ESRF - The European Synchrotron, 71, Avenue des Martyrs, 38000 Grenoble, France and Department of Physics, University of Warwick, Coventry CV4 7AL, UK.
[4] School of Mechanical & Aerospace Engineering, Queen's University Belfast, BT9 5AH, UK.
[5] International Institute for Nanocomposites Manufacturing (IINM), WMG, University of Warwick, Coventry, CV4 7AL, UK.

*Correspondence to: Ellen L. Heeley (E-mail: Ellen.Heeley@open.ac.uk)

Keywords

Polymer-MWCNT nanocomposites, crystalline morphology, kinetics, small- and wide-angle X-ray scattering (SAXS/WAXS), nanohybrid shish-kebab structure (NHSK)

Abstract

The combination of synchrotron Small- and Wide-Angle X-ray scattering (SAXS/WAXS), and thermal analysis was used to follow the evolution of crystalline morphology and crystallization kinetics in a series of melt-processed composites of poly(ethylene terephthalate) (PET) and multiwall carbon nanotubes (MWCNT). The as-extruded PET-MWCNT composites underwent both hot and cold isothermal crystallizations where a final oriented nanohybrid shish-kebab (NHSK) crystalline structure was observed. An oriented NHSK structure was seen to persist even after melting and recrystallization of the composites. From the scattering data, we propose a model whereby the oriented MWCNTs act as heterogeneous nucleation surfaces (shish) and the polymer chains wrap around them and the crystallites (kebabs) grow epitaxially outwards during crystallization. However, depending on crystallization temperature, unoriented crystallites also grow in the polymer matrix, resulting in a combination of a NHSK and lamellar morphology. In contrast, the neat PET homopolymer showed the sporadic nucleation of a classic unoriented lamellar structure under the same isothermal crystallization conditions. These results provide a valuable insight into

the distinctive modification of the crystalline morphology of melt-processed polymer-MWCNT composites prior to any secondary processing, having a significant impact on the use of MWCNTs as fillers in the processing and modification of the physical and mechanical properties of engineering polymers.

1. Introduction

The addition of multi-wall carbon nanotubes (MWCNTs) as functional fillers into commercially and industrially important engineering polymers, is well known to significantly improve their mechanical, electrical and thermal properties [1-8]. These properties are ultimately controlled in part by the polymer's crystalline morphology. However, critical to understanding and manipulating the improvements in physical properties of the polymer, the morphology development during processing of a polymer, needs to be efficiently monitored. Thus, providing invaluable information on how MWCNTs influence the nucleation and crystallization process of the homopolymer. Essentially, interpreting the morphology development in polymer-MWCNT composites during processing and correlating this with the mechanical and electrical properties, is of great importance in advancing the application and use of these composite materials [9]. However, the complex role that MWCNTs play in the morphology development in polymer composite systems during processing, is still poorly understood especially when applied to polymer melt systems.

Here, we focus our attention on the crystalline morphology development in MWCNT filled poly(ethylene terephthalate) PET [10], (an engineering polymer widely used in applications such as fibres, films, packaging, electronic components and circuits). Recently, we have shown that during uniaxial deformation of PET-MWCNT composites (at low loadings up to 4%wt), significant improvements in the mechanical and electrical properties and bulk crystallinity compared to the neat PET homopolymer, are observed [11,12]. Improvements in physical properties were directly linked to the MWCNT reinforcement and nucleating effects on the polymer matrix. The crystalline morphology that evolved during uniaxial deformation of the composites, indicated an oriented 'shish-kebab' type of structure commonly seen in polymers under deformation [13-15]. Here, the MWCNTs act as heterogeneous nucleation sites (or shish) where polymer chains wrap around them and then the crystallites (or kebabs) grow epitaxially outwards during crystallization. This has been termed a 'nanohybrid shish-kebab' (NHSK) morphology [16-21]. However, polymer-MWCNT composites can also form a *trans-crystalline* (TCL) structure, which has mainly

been observed during the solution-crystallization of poly(olefin)s and MWCNT fibres [20-24]. A TCL morphology, predominantly occurs where MWCNT mass fractions are high (up to 80% wt aggregating into fibres or arrays) and the polymer is crystallized from solution giving a compact layer on the surface of the MWCNT fibres and improved MWCNT dispersion [23,24]. Further to this, a hierarchal NHSK type of morphology was recently reported for electrospun poly($\mathcal{E}$-caprolactone)(PCL) - MWCNT composites, where a secondary 'nanofiber shish-kebab' (NFSK) crystalline morphology evolved after the incubation of the NHSK nanofibers in solution [25]. Similarly, a layered structure has been suggested in Nylon 11- MWCNT composites where a uniform crystalline layer of polymer forms prior to a NHSK structure [26].

The TCL and NHSK crystalline morphologies described above, have mainly been restricted to polyolefin based polymer systems during solution crystallization, that is, the polymer is grown on the surface of MWCNTs which are present as nanotubes in high concentrations or as aggregated fibres. However, this is not representative of commercial polymer processing techniques involving polymer melts where the concentrations of MWCNT fillers is usually less than 5% wt. Thus, there are few studies monitoring the crystalline structure evolution of engineering polymer systems such as polyesters prepared via melt mixing with low concentrations of MWCNTs. Recently, Cruz-Delgado [27], described the non-isothermal crystallization for PET-MWCNT composites (bulk polymer melts up to 2% wt), where they suggest the PET chains wrap around and orient on the MWCNTs due to aromatic π-π interactions. The crystallization kinetics revealed a confined crystallization process giving rod or disc-like crystallites. Similar results have been reported by Zhou [28], for PCL-MWCNT solution crystallized composites, where the initial helical wrapping of polymer chains act as nucleation points for crystallites to grow with random orientations – this can then straighten the MWCNT (depending on MWCNT diameter and length).

Several, studies showing the formation of lamellar, shish-kebab or NHSK morphologies have been reported for various polymer-MWCNT composites which have been under melt-shear processing (e.g. uniaxial deformation, injection moulding, melt spun fibres and shear flow) [12, 29-36]. In these studies, the MWCNTs are aligned with the polymer chains during processing (under shear flow), and so oriented NHSK morphologies are seen, where again the MWCNTs act as oriented nucleation sites for epitaxial crystallization. [12,16,18,37]

The growth and formation of a polymer-MWCNT NHSK morphology is dependent on several parameters, including MWCNT diameter, periodicity of the kebabs, lamellar thickness

and the processing conditions applied to the polymer-MWCNT composite. In a polymer matrix three crystalline growth scenarios are possible when filled with MWCNTs: (i) crystalline growth only occurs via nucleation on the MWCNT surface (NHSK morphology); (ii) nucleation sites occur exclusively in the polymer matrix; (iii) a combination of both.[36,38] Differentiating between these scenarios is difficult in polymer-melt composite systems and requires fast and sensitive techniques to follow the time-resolved morphology development during the polymers crystallization process. Recently, in a short communication [38], we reported some preliminary results of the hot isothermal crystallization in a set of melt processed PET-MWCNT composites with MWCNT loadings between 1 and 4 wt%. The MWCNTs were seen to act as heterogeneous nucleating surfaces (oriented shish structures) for the epitaxial growth of PET crystallites (kebabs) giving an oriented NHSK morphology. In contrast, the neat PET homopolymer showed the sporadic nucleation of a classic unoriented lamellar structure under the same isothermal crystallization conditions.

In this study, we present an extended and comprehensive set of data investigating the crystalline morphology development in melt processed PET-MWCNT composites as-extruded, prior to any further secondary processing. Here, synchrotron Small- and Wide-Angle X-ray scattering (SAXS/WAXS) and thermal techniques are employed allowing the time-resolved morphology, orientation and crystallization kinetics of the composites during both cold and hot isothermal crystallization conditions to be followed. Cold crystallizations were performed by heating the composites at temperatures above the glass transition temperature (T_g) of the composites [11], allowing the crystalline structure evolution of the as-extruded materials to be resolved, with respect to the MWCNT content and any residual molecular structure imposed by the extrusion process. Conversely, hot crystallizations were performed by first heating the composites above their melting temperature (T_m)[11], to erase any residual molecular and crystalline structure from the extrusion process, then quenched to the crystallization temperature. Again, allowing the crystalline morphology and kinetics to be followed in these materials. The results show unequivocally the role of the MWCNTs which not only act as nucleation surfaces for a NHSK-type crystallization, but due to residual orientation from the initial processing method any crystalline structure that evolves from the melt has a predisposed orientation. Hence, these results provide an invaluable insight into the distinctive modification of the crystalline morphology of melt-processed polymer-MWCNT composites prior to any secondary processing. This having a significant impact on the use of MWCNTs as functional fillers in the processing and modification of the physical and mechanical properties of engineering polymers.

2. Experimental

2.1 Materials

Commercial grade PET (Polyclear F019 (IV 0.895 dl/g) was supplied by Invista Resins & Fibers Gmbh. The multiwall carbon nanotubes (NANOCYL®, NC7000™ series), were produced in powder form, by catalytic carbon vapour deposition (CCVD). The MWCNTs had an average diameter of 9.5 nm and average length of 1.5 μm, a surface area of 250-300 $m^2\ g^{-1}$ and a carbon purity of 90%. A master-batch composite blend of PET and 10% MWCNTs, was diluted to give PET-MWCNT composites of 1 wt%, 2 wt% and 4 wt% loadings. The compounding and dilution process was achieved using a co-rotating intermeshing twin-screw extruder (Collin GmbH), with screw diameter of 25 mm and barrel length of 750 mm. The pre-dried (120 °C for 12 h), PET-MWCNT masterbatch was melt blended using a screw speed of 160 rpm and a residence time of 1 minute. The extruder barrel temperature settings over six zones from the feed zone were from 230 °C to 280 °C. The melt temperature in the die head was set at 260 °C.[11] The blends were cast extruded into sheets 100 mm wide and 1 mm thick. Samples will be referred to by the MWCNT wt% loading in PET; PET1%, PET2% and PET4% herein.

The dispersion of the MWCNTs in the PET matrix was confirmed by optical microscopy, SEM and TEM. The MWCNTs were confirmed to be well dispersed in the PET matrix with a small fraction aligned in the extrusion flow direction due to the design of the die used in the extrusion process.[11]

2.2 Thermal characterization

Thermal characterization using differential scanning calorimetry (DSC) of the neat PET and PET-MWCNT composites (post extrusion) was performed using a Perkin-Elmer DSC under an inert nitrogen gas atmosphere. Samples were subject to heating-cooling runs from 30 º to 300 º at a rate of 10 K min^{-1}. Table 1, lists the glass transition temperature (T_g), melting temperature (T_m), crystallization temperature (T_c) and crystallinity (X_c) of the composites from the DSC analysis. The percentage crystallinity X_c, of each sample was calculated from equation (1):

$$X_c = \frac{\Delta H_f}{\Delta H_f^0 (1-\phi)} \qquad (1)$$

where ΔH_f is the enthalpy of fusion from the integrated area under the melting transition from the DSC thermogram, ϕ is the weight fraction of MWCNTs in the PET homopolymer and ΔH_f^0 is the theoretical enthalpy change of 100% crystalline PET having a value of 117.6 J g^{-1}.[39]

Table 1. Thermal properties of PET and PET-MWCNT composites from DSC measurements.

Sample	T_g/°C	T_c/°C	T_m/°C	X_c/%
PET	85	194	254	28
PET1%	85	217	252	37
PET2%	85	220	252	35
PET4%	85	228	252	33

2.3 Synchrotron X-ray instrumentation and measurements:

Two-dimensional (2D) Small and Wide-Angle X-ray Scattering (SAXS/WAXS) measurements were performed on the XMaS (BM28) beamline at the European Synchrotron Radiation Facility (ESRF), France.[40] The X-ray energy used was 12.0 keV. 2D SAXS and WAXS data was collected on a MAR-CCD detector (calibrated with silver behenate), where the sample-to-detector distance was 340 mm for WAXS and 1500 mm for SAXS. A SAXS chamber flushed with helium was positioned between the sample position and detector reducing air scattering and absorption.

Samples were sealed in aluminium DSC pans fitted with mica windows (25 μm thickness, 7 mm Ø) and housed in a Linkam DSC600 heating stage positioned vertically in the incident X-ray beam before the SAXS chamber. Static 2D SAXS and WAXS data was collected for 20 s exposure time at temperatures of 30 °C and 270 °C. Time-resolved 2D SAXS data was obtained throughout isothermal crystallization experiments:

- Hot isothermal crystallizations; the samples were heated to 270 °C and held for 10 minutes (to erase any thermal history), then quenched at a rate of 50 K min^{-1}, to the desired crystallization temperature, between 210 ºC and 240 ºC.
- Cold isothermal crystallizations; samples were heated from room temperature at 50 K min^{-1} to the desired temperature, between 95 ºC and 130 ºC. In each case, SAXS data collection was started once the crystallization temperature was reached and continued throughout the crystallization process at a rate of

between 8 s and 15 s per frame depending on the isothermal crystallization temperature.

2.4 SAXS/WAXS data analysis

SAXS and WAXS data were normalized for sample thickness, transmission and background scattering. All X-ray data reduction and analysis was performed using and CCP13 FibreFix software.[41] The time-resolved 2D SAXS data were reduced to 1D intensity plots, $I(q, t)$, by sector averaging to a radius, q, where $q = (4\pi/\lambda) \sin(\theta)$, θ is the scattering angle and λ is the X-ray wavelength (1.03 Å). The invariant, Q_s, was then obtained from the 1D SAXS data where:

$$Q_s(t) = \int_0^{\infty} q^2 I(q,t)\mathrm{d}q \approx \int_{q_1}^{q_2} q^2 I(q,t)\mathrm{d}q \qquad (2)$$

The normalized Q_s data was used to follow the development of the isothermal crystallization process with respect to time, at each isothermal crystallization temperature. The crystallization curves were used to obtain the crystallization half-time, $t_{1/2}$, which represents the time taken to reach 50% conversion to full crystallinity at a specific temperature.

To estimate the relative molecular orientation from the 2D SAXS data, radial azimuthal 1D profiles were obtained from the angular variation in intensity, $I(q, \varphi)$, at a fixed radius q, over an azimuthal angle, φ, range of 0 - 360°. The 1D profiles of the azimuthal peaks were fitted using Gaussian functions to obtain the average full width at half maximum (FWHM) values.[12,38,42]

Avrami plots [43,44], using the double logarithmic from of the Avrami equation, were obtained for the isothermal crystallization measurements from Q_s:

$$\ln(\ln[1 - X_s(t)]) = n \ln t + \ln k \qquad (3)$$

where, the crystallinity $X_s(t) = Q_s(t)/Q_s(\infty)$, k is the crystallization rate constant and n is the Avrami exponent, being related to the nucleation process and the dimensionality of the growth unit during the crystallization process. Using the plots from Equation (2), values of n from the slope of the linear region of the plot and $\ln k$ from the intercept at $t = 1$, were obtained.

Correlation function analysis was performed on the 1D SAXS scattering profiles using a purpose written 1D correlation function software.[45] The correlation function, $\gamma(R)$, is expressed as:

$$\gamma(R) = \frac{1}{Q_s}\int_0^\infty I(q)q^2 \cos(qR)\mathrm{d}q \quad (4)$$

where $I(q)$ is the scattering intensity and Q_s from the 1D SAXS data from:

$$Q_s(t) = \int_0^\infty q^2 I(q)\mathrm{d}q \approx \int_{q_1}^{q_2} q^2 I(q)\mathrm{d}q \quad (5)$$

was obtained between the experimental limits of q_1 (the first real data point) and q_2 (the region where $I(q)$ is constant). To compute the correlation function from the 1D SAXS profiles, the data was extrapolated ($q \rightarrow \infty$) using a Porod [46], tail fit and a linear back extrapolation ($q \rightarrow 0$) was applied. Several parameters were extracted from the fitted correlation function which assumes an ideal two-phase lamellar morphology.[47] The long period, L_p, being the average dimension of a the crystalline and amorphous regions, L_c, the crystallite dimension and average bulk crystallinity, X_c, values were extracted from the correlation function for the final SAXS data frame from the isothermal crystallization process.[12,42]

2.5 High-resolution transmission electron spectroscopy, HRTEM

Each sample was cut into a square piece with dimensions of ca. 5 mm x 5 mm and thickness of ca. 0.8 mm and then inserted in to a cryo-microtome specimen holder and trimmed using a trimming blade (Trim 45) to a depth of 100 – 300 nm or until a shiny, reflective smooth surface was obtained. All samples were then sectioned using a Diamond Knife (cryo 35°, dry, 3.0 mm) to obtain film sections with thickness of ~50 nm. The film sections were then transferred onto 200 mesh TEM copper grids with Lacey carbon film. The sections were examined using a Jeol 2100 LaB6 TEM operating with an accelerating voltage of 80 – 200 kV (magnification up to ×100000).

3. Results and Discussion

Thermal characterization (Table 1), shows that on addition of MWCNTs to the polymer matrix there is no significant change in T_g and T_m. However, there is a marked difference in T_c (from 194 to 228 ºC), which increases with increasing MWCNT content, indicating that the MWCNTs act as heterogeneous nucleating agents as the PET crystallizes (i.e. increasing the crystallization kinetics). The crystallinity of the PET generally increases on

addition of MWCNTs, but it begins to fall slightly as more MWCNTs are added, this being attributed to a reduction in crystalline perfection even though the crystallization kinetics are increased and the difficulties in dispersing MWCNTs in polymer melts at higher loadings. [11,12]

Static SAXS was taken for the as-extruded samples to reveal any residual crystalline structure from the extrusion process. SAXS patterns of the extruded samples at 30 ºC prior to any further crystallization are given in Figure 1, including schematics of the associated polymer crystalline or amorphous structure. [12,42,48,49] The SAXS pattern for neat PET shows only diffuse scattering around the central beam stop, thus indicating no crystalline structure prevails from the extrusion process and the polymer is amorphous. In comparison, the PET1% composite shows increased scattering around the beam stop seen as a ring of intensity. This indicates that some crystalline lamellar structure had developed post extrusion. However, no obvious orientation in the SAXS is observed. The SAXS patterns for the PET2% and PET4% composites also show increased intensity around the beam stop, but this has some orientation indicated by the scattering intensity being concentrated in arcs. This indicates that an oriented residual crystalline structure exists in the polymer post extrusion.[12,38] This oriented crystalline structure is attributed to an oriented NHSK morphology, where due to the design of the extruder die head [11], the MWCNTs are initially aligned in the polymer melt during extrusion. The MWCNTs then act as nucleating sites during the extrusion casting and cooling process (once extruded), and so an initial crystalline structure develops compared with the amorphous neat PET.

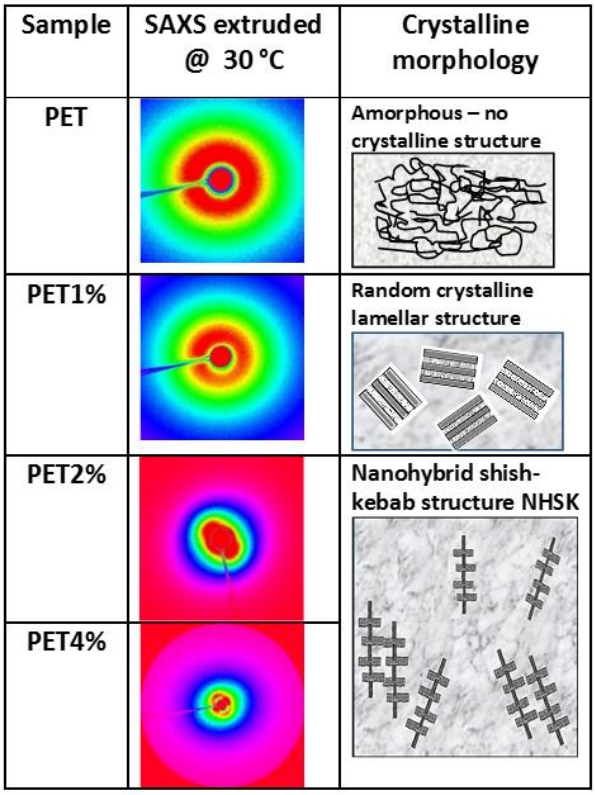

Figure 1: Static SAXS patterns for as extruded PET and PET-MWCNT composites and related crystalline morphology.

The residual orientation observed in the PET2% and PET4% composites, is likely to be due to the MWCNTs acting as rigid rod-like structures that do not relax in the viscous polymer matrix once aligned in the die head, thus their orientation is 'locked-in' once the polymer is extruded and cooled.[38]

The crystalline structure in the polymer composites is also confirmed with WAXS. Figure 2, shows static 2D WAXS patterns and corresponding 1D WAXS profiles for the PET and PET-MWCNT composites as extruded at 30 ºC. In Figure 2A, as in the SAXS, neat PET shows no crystalline Bragg rings, but diffuse scattering intensity around the beam stop, again confirming amorphous nature of the extruded polymer. The PET1% composite shows the PET (010) and ($0\bar{1}1$) triclinic [50], crystalline Bragg rings. The PET2% and PET4% composites also show these WAXS crystalline rings, which become sharper for the PET4% composite and tend to concentrate as arcs on the equator. The concentration of the (010) and ($0\bar{1}1$) rings on the equator, again verify that some preferred orientation in the crystalline structure is present, due to the extrusion process. In Figure 2B, 1D WAXS profiles show the development of the (010) and ($0\bar{1}1$) rings, where the ring breadth tends to reduce with increasing MWCNT content. This again indicating an increase in the crystalline structure in the composites. Note

that no difference in the crystalline lattice structure is seen (triclinic unit cell for neat PET), for the PET-MWCNT composites, suggesting that he MWCNTs are not incorporated in the PET crystalline lattice system [27,38].

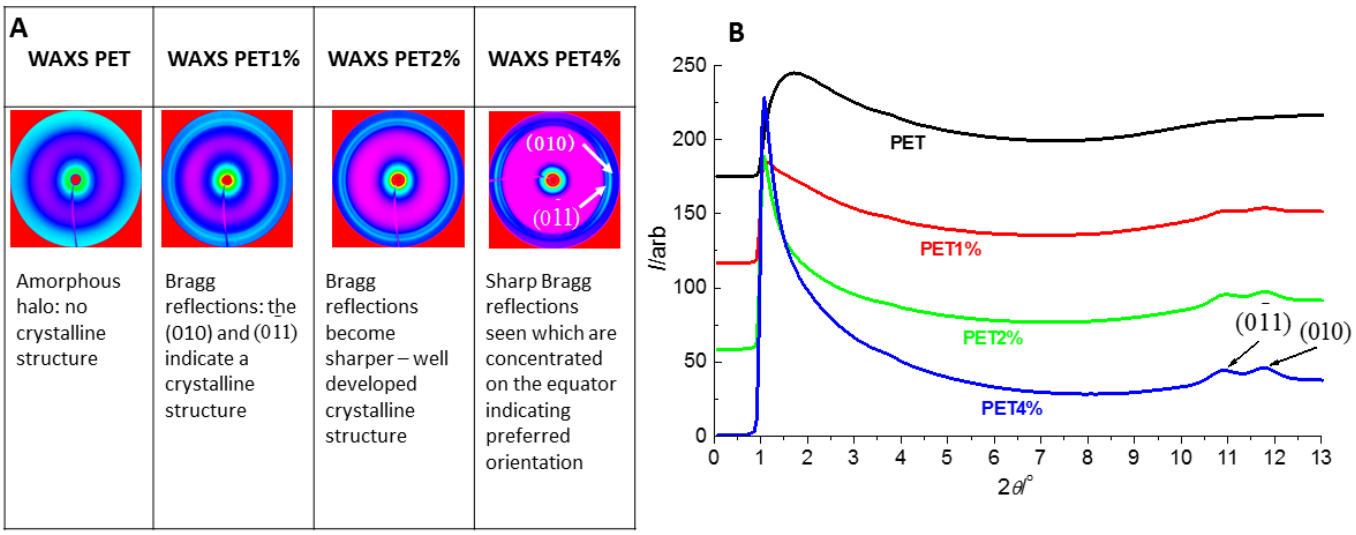

Figure 2: A: Static 2D WAXS patterns and B: corresponding 1D WXS profiles for extruded PET and PET-MWCNT composites.

The SAXS and WAXS patterns in Figures 1 and 2, for the as extruded PET and PET-MWCNT composites, indicate that the extrusion process induces orientation of the MWCNTs which in turn, act as heterogenous nucleating sites for crystallization to occur. This residual orientation increases with increasing MWCNT wt% in the PET composite.

To investigate the change in the initial structure of the neat PET and PET-MWCNT composites post extrusion, hot and cold isothermal crystallizations were performed. SAXS data was taken throughout the crystallizations to determine the morphology development, crystallization kinetics and type of crystallization process occurring in the PET and how the MWCNT influence theses parameters. Figure 3, shows the final 2D SAXS patterns at various isothermal crystallization temperatures once crystallization was completed. The final column in the figure shows the SAXS patterns of the melted samples at 270 °C. Samples were held at this temperature to erase any residual crystalline structure from the extrusion process, which is confirmed by the diffuse scattering around the beamstop. As the neat PET is crystallized at increasing cold isothermal temperatures (above T_g – 85 ºC), a ring of intensity clearly develops around the backstop, indicating a crystalline lamellar structure. (Note that no data is available for neat PET crystallized isothermally at 100 ºC as it took too long to crystallize within experimental time constraints.) In contrast, the PET-MWCNT composites all show the development of an oriented crystalline structure; this being observed as intense arc-like

scattering around the beam stop. The crystalline structure observed is that of an oriented NHSK morphology, as depicted in Figure 1. The residual crystalline structure from the extrusion process is not lost on further cold crystallization, but is perfected in the composites.

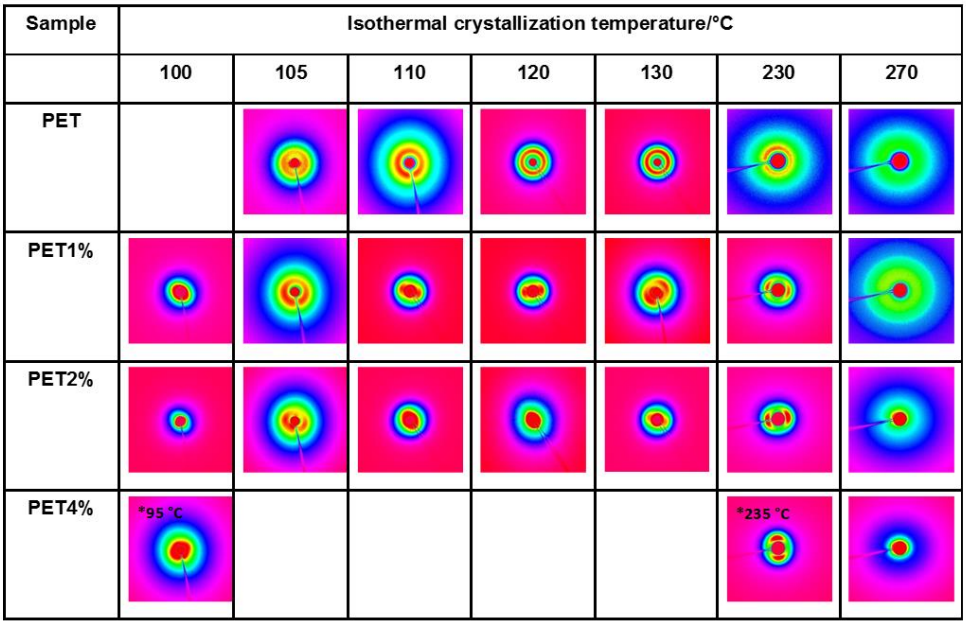

Figure 3: Final 2D SAXS patterns for neat PET and PET-MWCNT composites at various isothermal crystallization temperatures. Cold isothermal crystallization between 95 ºC – 130 ºC and hot crystallization at 230 ºC and 235 ºC. The final column shows SAXS of the neat PET and PET-MWCNT composites in the melt at 270 ºC.

Only one set of data is shown for the PET4% composite at an isothermal crystallization temperature of 95 ºC, as above this temperature, the crystallization kinetics were very fast and time constraints in data collection (detector frame rates), meant that the kinetics could not be followed effectively.

In column seven of Figure 3, 2D SAXS patterns are shown from the hot isothermal crystallizations at 230 ºC, for PET1 and PET2%, and 235 ºC for PET4%. This data was recently reported in a short communication [38], where during the hot crystallization process samples, were first heated above T_m to 270 ºC, to erase any crystalline structure from the extrusion process. The samples were then quenched to the crystallization temperature. The neat PET was seen to crystallize similarly to that during the cold crystallization temperatures; that is, forming a random lamellar structure. However, the PET-MWCNT composites all show that a very well defined oriented NHSK structure develops. This result is interesting as all residual polymer crystalline structure was originally erased at 270 ºC, but on cooling the

oriented NHSK structure returns. Again, the MWCNTs act as nucleating agents and their residual alignment from the extrusion process still persists in the re-melted polymer matrix. Thus, the MWCNTs act as a pre-aligned network of nucleation sites for PET crystallization.

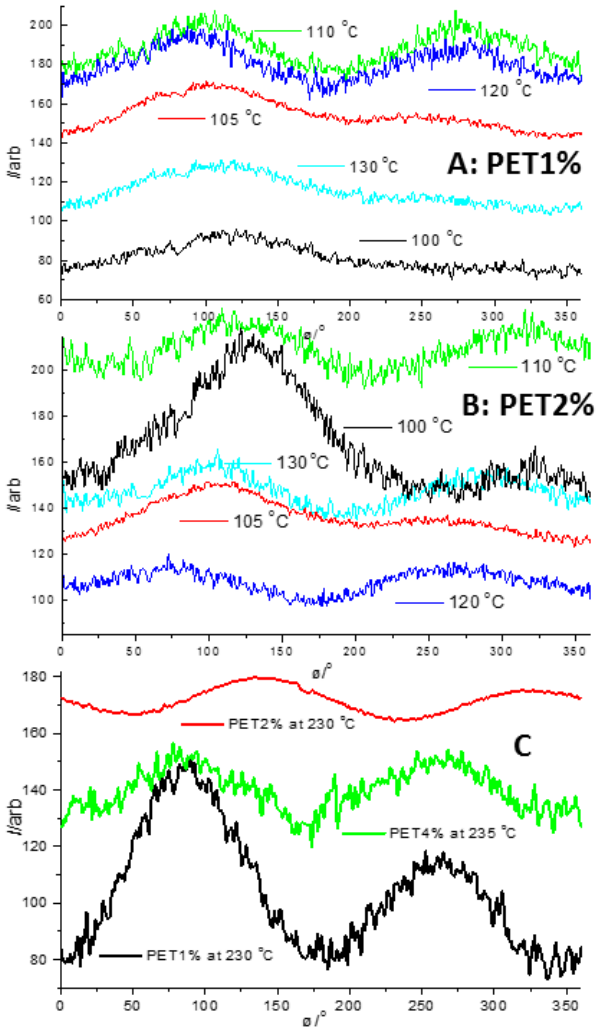

Figure 4: Example 1D Azimuthal profiles from final 2D SAXS patterns for: (A) PET1% and (B) PET2% at various cold crystallization temperatures (between 100 – 130 ºC). (C) 1D azimuthal profiles for PET1%, PET2% and PET4% composites at various hot isothermal crystallization temperatures (between 230 – 235 ºC).

To investigate the relative orientation of the 2D SAXS data at each isothermal crystallization temperature, radial 1D azimuthal profiles were taken. By way of example, 1D azimuthal profiles for the end of the isothermal crystallization process are shown in Figure 4, for the cold crystallized PET1% and PET2% composites (A and B), and (C) the hot crystallized PET1% - 4% composites. During cold isothermal crystallization the two peaks in the azimuthal intensity indicate some orientation is present. The two peaks are more pronounced as the cold crystallization temperature increases, indicating an increase in

orientation. For the samples, at 230 °C the azimuthal peaks are distinct. To quantify the orientation the average full-width half maximum (FWHM), was obtained from Gaussian fits of the azimuthal profiles [38], and plotted with respect to increasing isothermal crystallization temperature in Figure 5, for the PET-MWCNT composites.

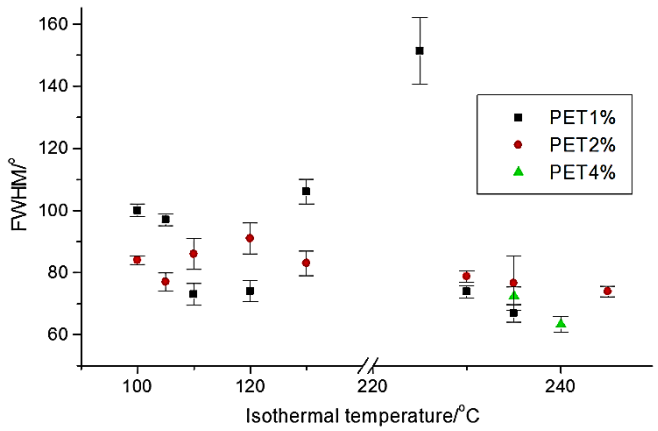

Figure 5. Change in FWHM with increasing isothermal crystallization temperature for the PET-MWCNT composites.

A reduction in the FWHM indicates an increase in orientation. For the cold crystallizations (between 100 - 130 ºC), there is little change in the orientation in the PET-MWCNT composites. In comparison for the hot crystallizations (between 230 – 245 ºC), the orientation tends to decrease slightly as the isothermal crystallization temperature decreases. However, it can be seen that overall, the orientation in the composites is greater from the hot crystallization process than from cold crystallizations. One outlier in the data is observed with the PET1% composite hot isothermally crystallized at 225 ºC, where the orientation is decreased significantly at this temperature. The decrease in the orientation can be explained by changes in the crystalline morphology. Initially, an oriented NHSK structure is seen in the samples during hot and cold crystallizations. This tends to be relatively constant during cold crystallizations where the oriented structure is already locked-in from the initial extrusion process. However, during hot isothermal crystallization the initial crystalline structure of the polymer is destroyed when heated and held above T_m [38]. Once quenched an oriented NHSK structure returns at temperatures where normally crystallization of the pure polymer would be very long (see crystallization kinetics section). As the hot isothermal crystallization temperature is decreased, the average orientation starts to decrease. This being due to the crystallization of the polymer matrix (in addition to the NHSK structure), giving more

crystallites with random orientations. This is evident with the PET1% composite at 225 ºC, where crystallization occurs in the polymer matrix (unoriented lamellar crystallization), at the lower temperature reducing the average orientation.

The morphology and crystallization kinetics during the hot and cold crystallizations were also obtained from the 1D radial profiles. The 1D radial profiles provided the normalised scattering invariant Q_s, allowing the crystallization process to be followed and the half-time, $t_{1/2}$, to be extracted. Figure 6, shows selected hot and cold isothermal crystallization curves for neat PET and each PET-MWCNT composite.

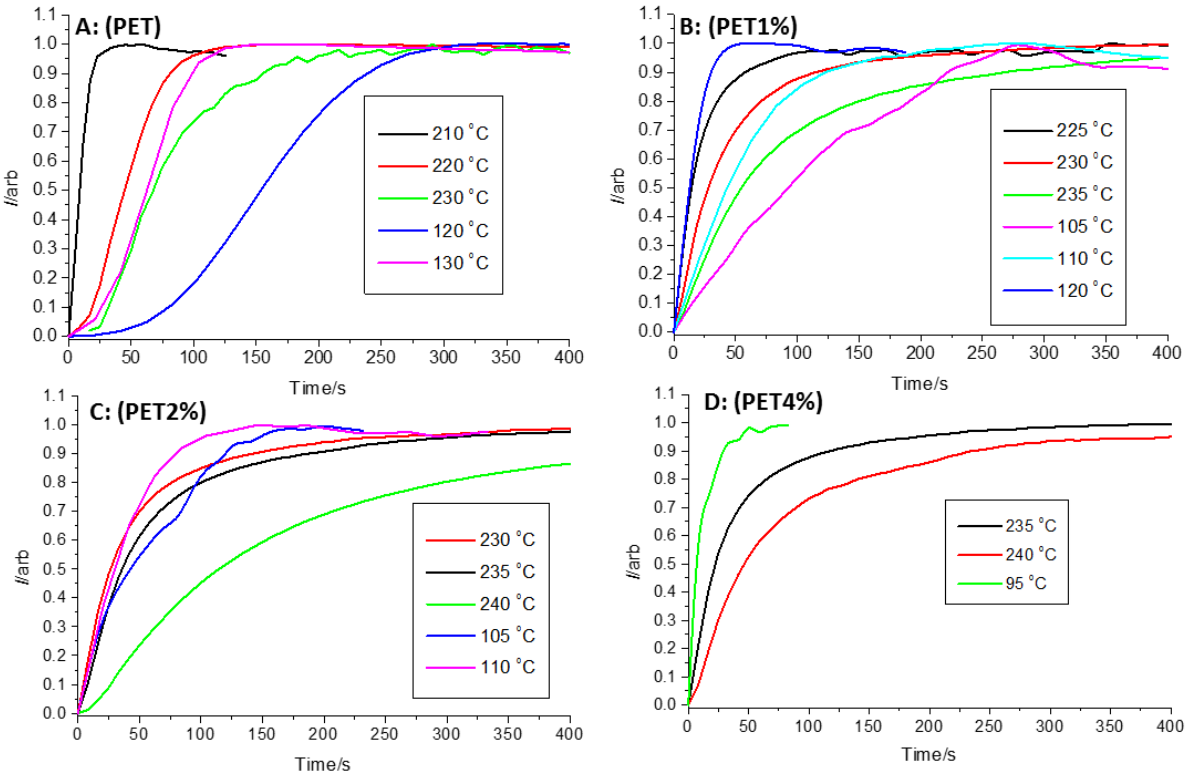

Figure 6. Hot and cold isothermal crystallization data obtained from the scattering invariant Q_s for (A): neat PET; (B): PET1%; (C): PET2% and (D) PET4%.

The hot and cold crystallization kinetics of neat PET were very slow at temperatures lower than 120 °C and higher than 230 °C, so are not shown in this figure. However, the addition of MWCNTs as nucleating agents means that the PET-MWCNT composites crystallize at lower and high temperatures, compared to the neat PET. Increasing the MWCNT content in the PET increases the crystallization kinetics dramatically, for example PET4% (Figure 6D), crystallizes too fast to follow reliably above 95 °C and below 235 °C.

Figure 7, shows the values of $t_{1/2}$, extracted from the crystallization curves in Figure 6. Here, this data reiterates the nucleating affect and thus increased crystallization kinetics the addition of MWCNTs have on PET, enabling the polymer to crystallize at low temperatures (above T_g) and high temperatures quenched from T_m, where the neat polymer would not normally crystallize within experimental time limits.

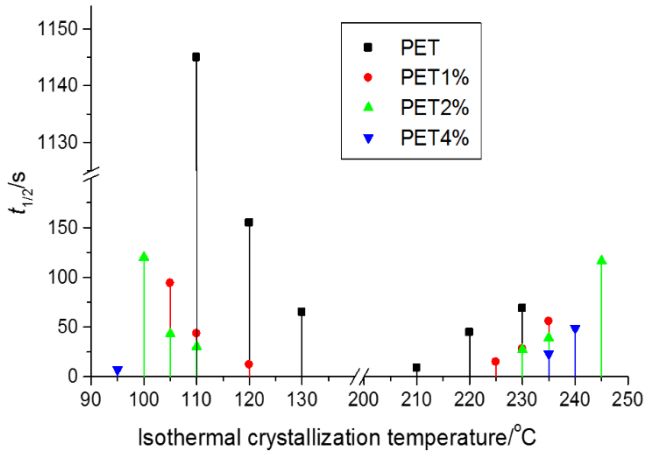

Figure 7. Crystallization half-times, $t_{1/2}$, from the hot and cold crystallization curves of neat PET and PET-WMCNT composites. Drop lines are shown to each temperature.

To determine information about the type of crystal growth Avrami analysis was performed on the cold and hot isothermal crystallization curves (in Figure 6). Double log plots were obtained (applying Equation (3)) and from these the values of n from the fitted slope of the linear region of the plot and ln k from the intercept at t = 1, were extracted. Examples of the Avrami double log plots for cold and hot crystallization of neat PET and PET-MWCNT composites at various temperatures are given in Figure 8.

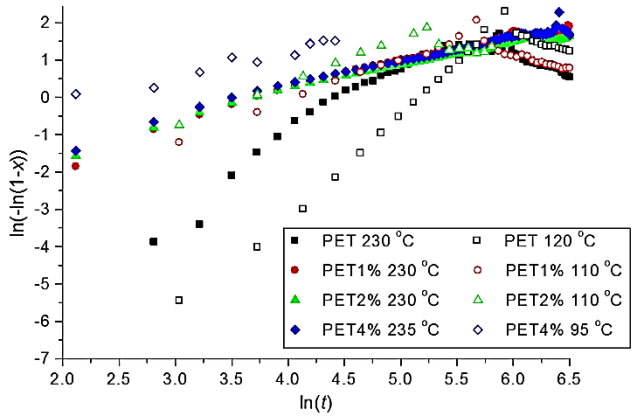

Figure 8. Selected Avarmi plots for the cold and hot isothermal crystallizations of PET and PET-MWCNT composites.

The extracted data from the linear fit of the Avrami plots and values of $t_{1/2}$ for the hot and cold crystallizations are collated in Table 2. The Avrami exponent *n*, for neat PET during cold and hot isothermal crystallization ranges from around 1.5 - 2.9. A value of 2.9 indicates a 2D disk shaped growth unit from sporadic nucleation sites.[27,38,51-53] The value of *n* decreases as the cold crystallization temperature increases, or as the hot crystallization temperature decreases, this is most likely due to the increased kinetics at these temperatures (see decrease in $t_{1/2}$ and increase in ln *k*), so the crystalline grow unit is less well formed (less perfect). This also correlates well with the SAXS data, where a randomly oriented lamellar crystalline structure develops. In contrast, the PET-MWCNTs show values of *n* tending to unity. This indicates a rod-like crystalline growth unit from instantaneous heterogeneous nucleation sites [27,38,51-53]. Again, this is supported by the SAXS data, where an oriented NHSK prevails for the composites and the MWCNT act as heterogeneous nucleation sites.

Table 2. Crystallization half-times $t_{1/2}$, Avrami exponent, *n*, and Avrami rate constant ln *k*, for the cold and hot isothermal crystallizations of PET and PET-MWCNT composites.

Sample	T_i/°C	$t_{1/2}$/s	**Avrami exponent, *n***	**ln(k/s^{-1})**
PET	120	155	2.9	-14.9
	130	65	2.6	-11.1
	210	9	1.5	-2.8
	220	45	2.0	-8.0
	230	69	2.7	-11.5
PET1%	105	94	1.3	-6.1
	110	43	1.0	-4.4
	120	12	1.0	-2.3
	225	15	0.8	-2.2
	230	28	0.9	-3.4
	235	56	1.0	-4.5
PET2%	105	43	1.4	-6.0
	110	30	1.2	-4.4
	230	27	0.9	-3.2
	235	39	0.9	-3.7
	245	116	1.2	-5.6
PET4%	95	7	0.8	-2.1
	235	23	0.7	-2.6
	240	49	1.0	-4.1

Further details of the crystalline morphology from the 1D SAXS data was obtained using correlation function analysis. Correlation functions were performed on the final 1D SAXS data frame of the hot and cold isothermal crystallization process for each sample. This

allowed the long period, L_p (average crystalline and amorphous repeat distance), L_c, the crystallite thickness and the bulk percentage crystallinity to be obtained at each crystallization temperature. Figure 9A, shows an example of the correlation function extracted from the 1D SAXS profile (inset), for neat PET crystallized at 130 °C. Figure 9B-D, shows plots of the extracted values of L_p, L_c and bulk percentage crystallinity with increasing isothermal crystallization temperatures, for all the PET and PET-MWCNT composites. There is little change in L_p (Figure 9B) for PET and the PET-MWCNT composites when cold crystallized (between 100 – 130 °C), but neat PET shows an overall smaller L_p than the composites. The crystallite size L_c (Figure 9C), increases for neat PET and the composites with increasing cold crystallization temperature, but as there is no significant change in L_p, therefore crystallites grow consuming the amorphous regions. This is mirrored in the general increase in percentage crystallinity during cold crystallizations (Figure 9D).

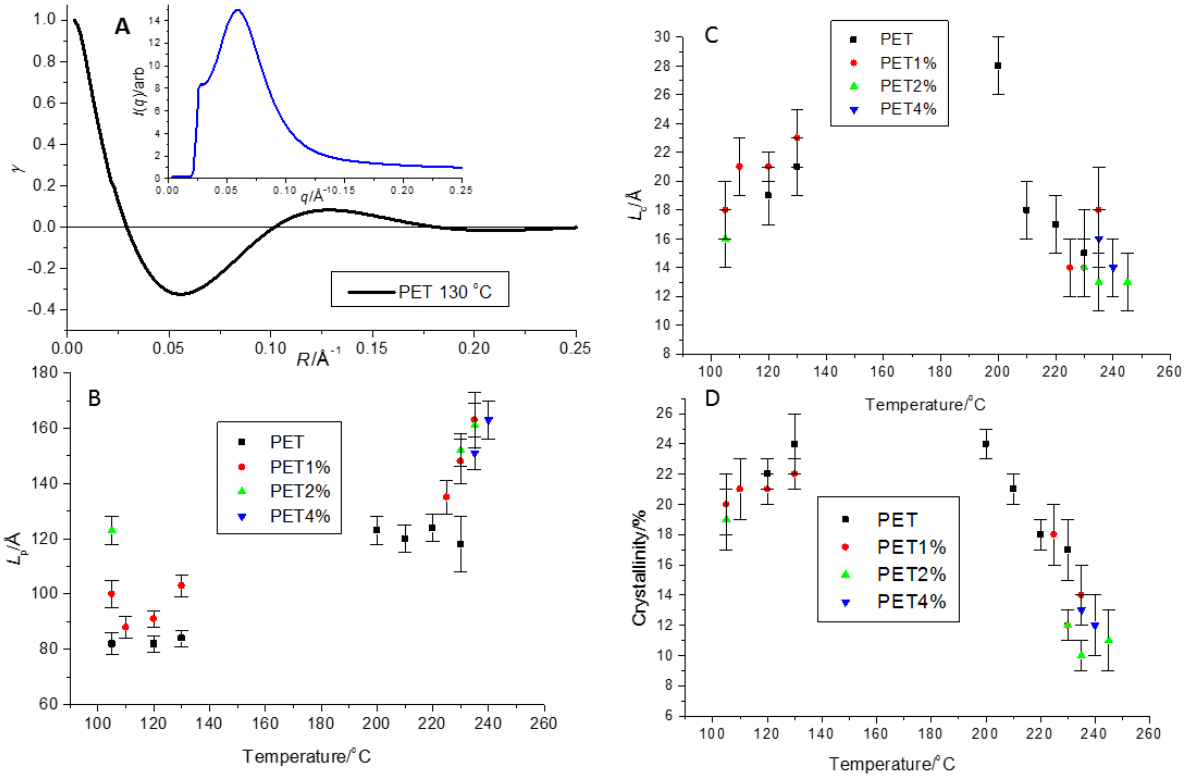

Figure 9. (A) Example correlation function profile for near PET isothermally crystallized at 130 °C (inset shows the 1D SAXS profile that the correlation function was calculated from). (B) Final long period, L_p, (C) final crystallite thickness L_c, and (D) final bulk percentage crystallinity for all samples with increasing isothermal crystallization temperature.

During the hot isothermal crystallizations (between 200 – 245 °C), the L_p of neat PET is again relatively constant, but the crystallite size L_c, increases as the crystallites grow into the amorphous regions and perfect as the crystallization temperature decreases. Hence, the

bulk crystallinity also increases with decreasing crystallization temperature. In contrast, the L_p for the PET-MWCNT composites tends to decrease as the hot crystallization temperature decreases, but L_c does not change significantly. The crystallinity also increases with decreasing crystallization temperature. This suggests that narrow crystallites are inserted into the amorphous regions, reducing the periodicity and hence increasing the bulk crystallinity.

Finally, HRTEM images were taken to verify the dispersal of the MWCNTs in the PET matrix after cold crystallization. Figure 10, shows the HRTEM images of the PET2% sample with increasing magnification. Here, the MWCNTs are well dispersed in the polymer matrix and show some preferred orientation. [11] As the magnification is increased (left to right) the MWCNTs appear to be embedded in the polymer matrix and coating of the MWCNTs by the polymer occurs, confirming crystallization of the polymer on the MWCNT surface. Similar results have been reported during the non-isothermal crystallization of PET-MWCNT at low cooling rates.[27]

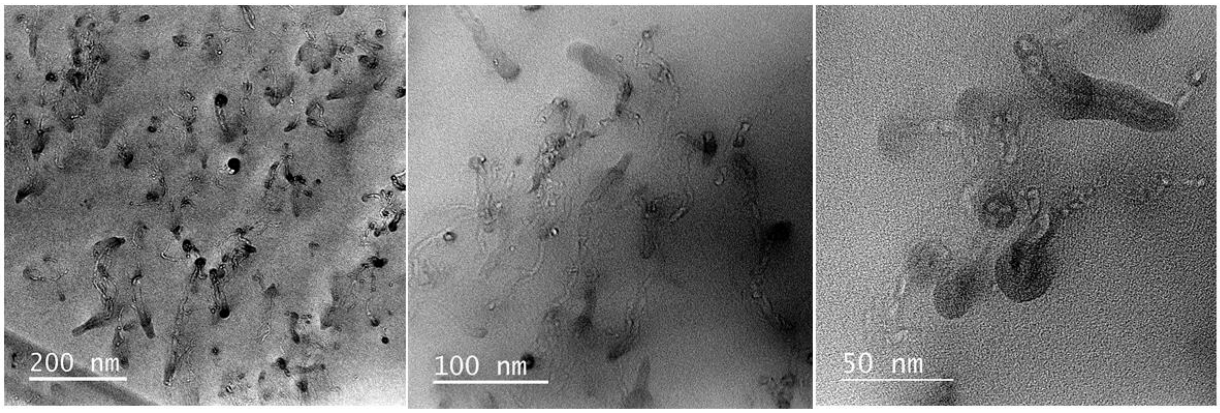

Figure 10. HRTEM images of cold crystallized PET2% with increasing magnification.

The combination of DSC, SAXS/WAXS and TEM techniques have given detailed insight into the role of MWCNT fillers during the isothermal hot and cold crystallization of PET. From the results presented here, it is apparent that on the addition of MWCNTs to PET, the resulting crystalline morphology, orientation, crystallization kinetics and crystallinity of the homopolymer are significantly altered. These changes are attributed to the heterogeneous nucleating effect of the MWCNTs. The SAXS/WAXS data revealed that there is pre-orientation of the MWCNTs from the extrusion process which provides pre-aligned nucleating surfaces for the PET molecular chains to align onto and then crystallize, resulting in a crystalline oriented structure. However, this was not observed for the neat PET, as the extrusion process did not align the PET chains and so an initial amorphous structure was obtained. Only on further isothermal crystallization of the neat polymer above T_g, does a

crystalline structure develop. Further to this, different crystalline structures develop during the cold and hot isothermal crystallization of the PET-MWCNTs composites.

We have assigned the crystalline morphology in the PET-MWCNT composites to a NHSK structure and propose a model for its formation under the different crystallization conditions (hot or cold crystallization). A schematic of the model is given in Figure 11. Figure 11A, shows the residual oriented crystalline morphology in the PET-MWCNT composites after extrusion, where a NHSK structure is observed, but some initial small crystallites are seen in the polymer amorphous matrix. Increasing the cold isothermal crystallization temperature for the composites (Figure 11B), the crystallite size and crystallinity increases (see Figure 9C-D), due to the thickening of the NHSK structures and some further crystallites developing in the polymer matrix.

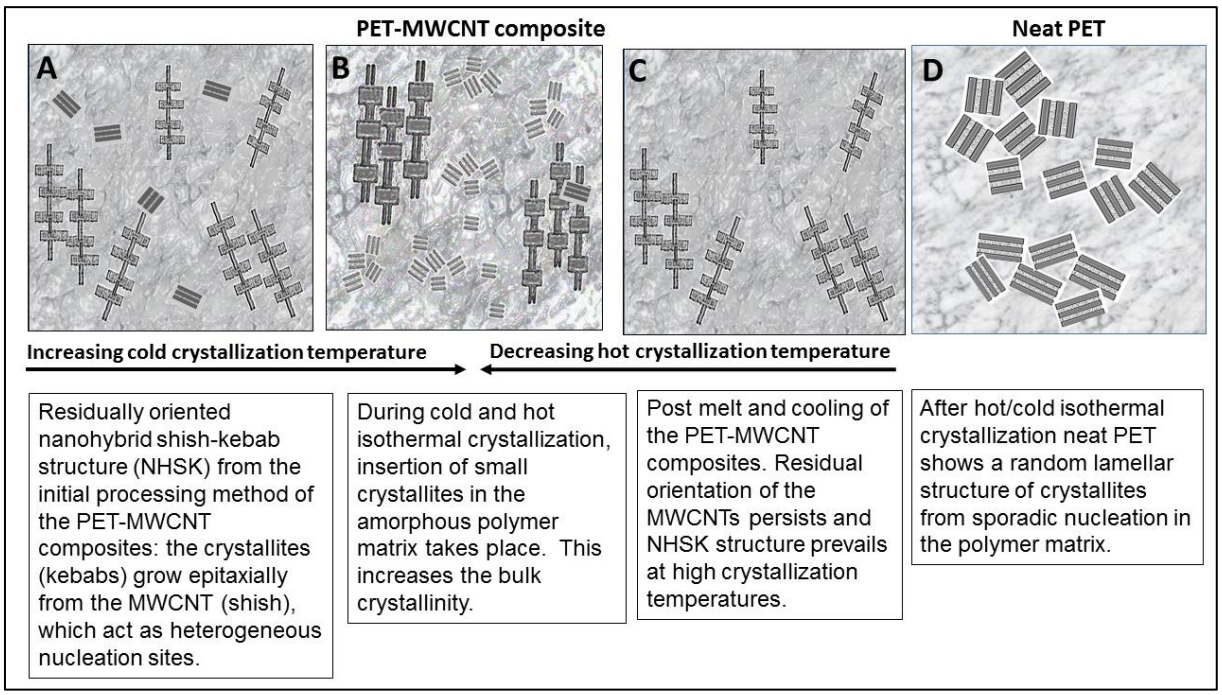

Figure 11. Morphology evolution during cold and hot isothermal crystallization in PET and PET-MWCNT composites. (A): residually oriented crystalline NHSK structure from the cast extrusion process of the PET-MWCNT composites. (B): insertion of lamellae into polymer matrix during increasing cold and decreasing hot isothermal crystallization of PET-MWCNT composites. (C) Post melt and cooling of PET-MWCNT composites where the oriented NHSK structure persists on hot crystallization. (D): Comparative random lamellar structure in neat PET after hot and cold isothermal crystallization.

Figure 11C, shows the NHSK structure once the composite had been melted (to remove any thermal history and crystalline structure), quenched below T_m and then hot isothermally crystallized. The MWCNTs retain their orientation from the initial extrusion process and so

an oriented NHSK structure prevails as the polymer re-crystallizes. Again, as the hot isothermal crystallization temperature is decreased the structure changes to that seen in Figure 11C, where new crystallites begin to insert and grow in the polymer matrix, increasing the crystallinity. Finally, Figure 11D, shows the crystalline structure that develops during both cold and hot isothermal crystallizations for neat PET, where an unoriented lamellar morphology develops via sporadic nucleation in the polymer matrix.

The model presented in Figure 11, shows how the addition of MWCNTs during hot and cold isothermal crystallization of PET influences crystalline morphology development. The MWCNTs undoubtedly act as nucleating surfaces for the crystallization of the polymer chains, therefore increasing the crystallization kinetics and ultimately this yields a NHSK structure. Also, any pre-orientation of the MWCNTs initially induced by the extrusion process is not removed on re-melting of the polymer matrix, that is, the MWCNTs do not relax into a random network in the viscous polymer melt so still act as pre-aligned nucleation sites during hot isothermal crystallizations, again producing an oriented NHSK structure.

Conclusions

Here, the combined use of SAXS/WAXS, thermal(DSC), and microscopy (HRTEM), techniques have given detailed information not only on the crystalline morphology, but crystallization kinetics in a set of PET-MWCNT nanocomposites when compared with neat PET. The scattering data has confirmed that an NHSK structure dominates in the PET-MWCNT composites, with the morphology and crystallization kinetics being controlled by the residual orientation of the MWCNTs in the polymer matrix. In contrast, an unoriented lamellar structure is observed in the neat PET when crystallized. The unoriented lamellar and NHSK morphologies of the PET and PET-MWCNT composites respectively, were further verified from the type of crystal growth and nucleation process obtained during the hot isothermal crystallizations, that is, sporadic nucleation of 2D disc shaped growth units in neat PET, compared with a heterogeneously nucleated rod-like growth units in the PET-MWCNT composites.

The results presented give an advanced understanding of the role of MWCNTs in the modification of the crystalline morphology as a consequence of melt mixing with PET prior to secondary processing. During initial extrusion of the polymer composites, the MWCNTs reinforce the polymer matrix, and in turn, act as oriented nucleation sites for the polymer chain to attach to and crystallize. Thus, a crystalline morphology is already present in the composites compared with the amorphous structure of the homopolymer. The validation of

the residual crystalline structure in the PET-MWCNT composites has a significant impact on further processing of these composites as well as the final physical and mechanical properties of the composite material.

Acknowledgements

X-ray beamtime at the ESRF was provided under the experimental application 28-01/1127. We are grateful for the assistance of all the EPSRC funded ESRF BM28 (XMaS) beamline staff and BM26 (DUBBLE) beamline for loan of instrumentation.

References

[1] O. Breuer, U. Sundararaj, Big returns from small fibers: A review of polymer/carbon nanotube composites, Polymer composites, 25 (2004) 630-645.

[2] J.N. Coleman, U. Khan, W.J. Blau, Y.K. Gun'ko, Small But Strong: A Review of the Mechanical Properties of Carbon Nanotube-Polymer Composites, Carbon, 44 (2006) 1624-1652.

[3] R. Khare, S. Bose, Carbon Nanotube Based Composites- A Review, Journal of Minerals and Materials Characterization and Engineering, 4 (2005) 31-46.

[4] Z. Spitalsky, D. Tasis, K. Papagelis, C. Galiotis, Carbon nanotube–polymer composites: Chemistry, processing, mechanical and electrical properties, Progress in polymer science, 35 (2010) 357-401.

[5] T. McNally, P. Pötschke, Polymer-carbon nanotube composites: Preparation, properties and application, Cambridge United Kingdom: Woodhead Publishing, 2011.

[6] B.P, Grady, Carbon nanotube-polymer composites manufacture, properties, and applications, 1st Ed. Wiley-Interscience: New York, 2011.

[7] G. Pandey, E.T. Thostenson, E. T. Carbon Nanotube-Based Multifunctional Polymer Nanocomposites. Polymer Reviews, 52 (2012) 355-416.

[8] B. Arash, Q. Wang, V.K. Varadan, Mechanical properties of carbon nanotube/polymer composites, Sci. Rep. 4, (2014) 6479.

[9] J.M. Wernik, S.A. Meguid, Appl. Mech. Rev., Recent developments in multifunctional nanocomposites using carbon nanotubes, 63 (2010) 050801-0508037.

[10] J. Y. Kim, S.H. Kim, In High Performance PET/Carbon Nanotube Nanocomposites: Preparation, Characterization, Properties and Applications, Nanocomposites - New Trends and Developments, Ebrahimi, F., Ed.; InTech, 2012, Chap. 5. DOI: 10.5772/50413.

[11] B. Mayoral, P.R. Hornsby, T. McNally, T.L. Schiller, K. Jack, D.J. Martin, Quasi-solid state uniaxial and biaxial deformation of PET/MWCNT composites: structural evolution, electrical and mechanical properties, RSC Adv. 3 (2013) 5162-5183.

[12] E. L. Heeley, D. J. Hughes, E. Crabb, M. Kershaw, O. Shebanova, S. Leung, B. Mayoral, T. McNally, Structure evolution in polyethylene terephthalate (PET) - multi-walled carbon nanotube (MWCNT) composite films during in-situ uniaxial deformation, Polymer 92 (2016) 239-249.

[13] Keller A.; Willmouth F. M., Some macroscopic properties of stirring-induced crystals of polyethylene, *J. Macromol. Sci*., B6 (1972) 493-537.

[14] I.M. Ward, 'Structure and properties of oriented polymers', Wiley, New York, 1975.

[15] A. Keller, H.W. Kolnaar, Flow Induced Orientation and Structure Formation. In Processing of Polymers, Meijer, H. E. H., Ed.; 1997, VCH; New York, 187.

[16] C. Y Li, L. Li, W. Cai, S.L. Kodjie, K.K. Tenneti, Nanohybrid Shish-Kebabs: Periodically Functionalized Carbon Nanotubes, Adv. Mater., 17 (2005) 1198-1202.

[17] L. Li , C. Y. Li , C. Ni. Polymer crystallization-driven, periodic patterning on carbon nanotubes, J. Am. Chem. Soc., 128 (2006) 1692–1699.

[18]. L. Li, B. Li, M.A. Hood, C. Y. Li, Carbon nanotube induced polymer crystallization: The formation of nanohybrid shish–kebabs, Polymer, 50 (2009) 953-965.

[19] L. Li, W. Wang, E. D. Laird, C. Y. Li, M. Defaux, D.A. Ivanov, Polyethylene/carbon nanotube nano hybrid shish-kebab obtained by solvent evaporation and thin-film crystallization, Polymer, 52, (2011), 3633-3638.

[20] E.D. Laird, C.Y Li, Structure and Morphology Control in Crystalline Polymer–Carbon Nanotube Nanocomposites, Macromols, 46 (2013) 2877-2891.

[21] L. Zhang, T. Tao, C. Li, Formation of polymer/carbon nanotubes nano-hybrid shish–kebab via non-isothermal crystallization, Polymer, 50 (2009) 3835–3840.

[22] S.J. Zhang, M. L. Minus, L. Zhu, C.P. Wong, S. Kumar, Polymer transcrystallinity induced by carbon nanotubes, Polymer, 49 (2008) 1356-1364.

[23] S. Zhang, W. Lin, C-P. Wong, D. G. Bucknall, S. Kumar, Nanocomposites of carbon nanotube fibers prepared by polymer crystallization, ACS Applied Materials & Interfaces, 2 (2010) 1642-1647.

[24] S. J. Zhang, W. Lin, X. W. Lin, C. P. Wong, S. Z. D. Cheng, D. Bucknall, Surface-induced crystallization in high volume fraction aligned carbon nanotube polymer composites, Macromolecular Chemistry and Physics, 211 (2010) 1003-1011.

[25] M. M. L. Arras, R. Jana, M. Mühlstädt, S. Maenz, J. Andrews, Z. Su, C. Grasl, K. D. Jandt, In Situ Formation of Nanohybrid Shish-Kebabs during Electrospinning for the Creation of Hierarchical Shish-Kebab Structures, Macromolecules, 49 (2016) 3550-3558.

[26] M. Nie, Di. M. Kalyon, F.T. Fisher, Interfacial Load Transfer in Polymer/Carbon Nanotube Nanocomposites with a Nanohybrid Shish Kebab Modification, ACS Appl. Mater. Interfaces, 6 (2014) 14886-14893.

[27] V. J. Cruz-Delgado, C.A. Ávila-Orta, A.B. Espinoza-Martínez, J.M. Mata-Padilla, S.G. Solis-Rosales, A.F. Jalbout, F.J. Medellín-Rodríguez, B. S. Hsiao, Carbon nanotube surface-induced crystallization of polyethylene terephthalate (PET), Polymer, 55 (2014) 642-650.

[28] B. Zhou, J-H Li, B. Fan, P. Li, J-T. Xu, Z-Q. Fan. Straight and Rod-like Core–Sheath Crystals of Solution-Crystallized Poly(ε-caprolactone)/Multiwalled Carbon Nanotube Nanocomposites, Cryst. Growth Des., 16 (2016) 6817–6827.

[29] S. Mazinani,S, A. Ajji, C. Dubois, Structure and properties of melt-spun PET/MWCNT nanocomposite fibers, Polym. Eng. Sci. 50 (2010) 1956-1968.

[30] J.Y. Kim, H.S. Park, S.H. Kim, Multiwall-carbon-nanotube-reinforced poly(ethylene terephthalate) nanocomposites by melt compounding, J.Appl. Polym. Sci., 103 (2007) 1450–1457.

[31] S. Tzavalas, V. Drakonakis, D.E. Mouzakis, D. Fischer, V.G. Gregoriou, Effect of Carboxy-Functionalized Multiwall Nanotubes (MWNT−COOH) on the Crystallization and Chain Conformations of Poly(ethylene terephthalate) PET in PET−MWNT Nanocomposites, Macromols, 39 (2006) 9150-9156.

[32] T. Vad, J. Wulfhorst, T-T. Pan, W. Steinmann, S. Dabringhaus, M. Beckers, G. Seide, T. Gries, W.F.C. Sager, M. Heidelmann, T.E. Weirich, Orientation of Well-Dispersed Multiwalled Carbon Nanotubes in Melt-Spun Polymer Fibers and Its Impact on the Formation of the Semicrystalline Polymer Structure: A Combined Wide-Angle X-ray Scattering and Electron Tomography Study, Macromols, 46 (2013) 5604-5613.

[33] P. Patil, L. Balzano, G. Portale, S. Rastogi, Influence of shear in the crystallization of polyethylene in the presence of SWCNTs, Carbon, 48 (2010) 4116-4128.

[34] P. Liu, K.L. White, H. Sugiyama, J. Xi, T. Higuchi, T. Hoshino, R. Ishige, H. Jinnai, A. Takahara, A.; H-J. Sue, Influence of Trace Amount of Well-Dispersed Carbon Nanotubes on Structural Development and Tensile Properties of Polypropylene, Macromols, (46) 2013 463-473.

[35] J. Yang, C. Wang, K. Wang, Q. Zhang, F. Chen, R. Du, Q. Fu, Direct Formation of Nanohybrid Shish-Kebab in the Injection Molded Bar of Polyethylene/Multiwalled Carbon Nanotubes Composite, Macromols., 42 (2009) 7016-7023.

[36] A. Wurm, D. Lellinger, A.A. Minakov, T. Skipa, P. Pötschke, R. Nicula, I. Alig, C. Schick, Polymer, 55 (2014) 2220-2232.

[37] Y. H. Chen, G. J. Zhong, J. Lei, Z. M. Li, B. S. Hsiao, In Situ Synchrotron X-ray Scattering Study on Isotactic Polypropylene Crystallization under the Coexistence of Shear Flow and Carbon Nanotubes, Macromols, 44 (2011) 8080-8092.

[38] E. L. Heeley, D.J. Hughes, E.M. Crabb, J. Bowen, O. Bikondoa, B. Mayoral, T. McNally, Confirmation of a nanohybrid shish-kebab (NHSK) structure in composites of PET and MWCNTs, J. Polym. Sci., Part B: Polym. Phys. 55 (2017) 132-137.

[39] A. Metha, U. Gaur, B. Wunderlich, Equilibrium melting parameters of poly(ethylene terephthalate), J. Polym. Sci., Polym.Phys. Ed., 16 (1978) 289-296.

[40] XMaS: The UK Materials Science Facility at the ESRF. http://www2.warwick.ac.uk/fac/cross_fac/xmas/ (Assessed 30/01/2017)

[41] FibreFix http://www.diamond.ac.uk/Beamlines/Soft-Condensed-Matter/small-angle/SAXS-Software/CCP13/FibreFix.html (Assessed 30/01/2017)

[42] E.L. Heeley, T. Gough, D.J. Hughes, W. Bras, J. Rieger, A.J. Ryan, Effect of processing parameters on the morphology development during extrusion of polyethylene tape: An in-line small-angle X-ray scattering (SAXS) study, Polymer, 54 (2013) 6580-6588.

[43] M. Avrami, Kinetics of Phase Change. I General Theory, J. Chem. Phys., 7 (1939) 1103-1112.

[44] M. Avrami,. Kinetics of Phase Change. II Transformation ‐ Time Relations for Random Distribution of Nuclei, J. Chem. Phys., 8 (1940) 212 -224.

[45] Simple SAXS and WAXS Software written in Excel. http://coecs.ou.edu/Brian.P.Grady/saxssoftware.html#Allprograms (Assessed 30/01/2017)

[46] G. Porod, Die Röntgenkleinwinkelstreuung von dichtgepackten kolloiden Systemen, *Kolloid Z*, 124 (1951) 83-114.

[47] F. J. Baltá-Calleja, G. G. Vonk , X-ray scattering of synthetic polymers, Elsevier Science, New York, 1989.

[48] S. Röber, P. Bösecke, H. G. Zachmann, Small angle X-ray scattering pole figures of semicrystalline polymers obtained by synchrotron radiation, Makromol. Chem. Macromol. Symp., 15 (1988) 295-310.

[49] A. I. Abou-Kandil, A. H. Windle, The development of microstructure in oriented polyethylene terephthalate (PET) during annealing, Polymer, 48 (2007) 5069-5079.

[50] R. de P. Daubeny, C. W. Bunn, C. J. Brown, The Crystal Structure of Polyethylene Terephthalate, Proc. R. Soc. Lond. A, 226 (1954) 531-542.

[51] X. F. Lu, J. N. Hay, Isothermal crystallization kinetics and melting behaviour of poly(ethylene terephthalate), Polymer, 42, (2001)9423-9431.

[52] G. Antoniadis, K.M. Paraskevopoulos, D. Bikiaris, K. Chrissafis, Melt-crystallization mechanism of poly(ethylene terephthalate)/multi-walled carbon nanotubes prepared by in situ polymerization, J. Polym. Sci. B Polym. Phys., 47 (2009) 1452-1466.

[53] A. Al-Mulla, Isothermal crystallization kinetics of poly (ethylene terephthalate) and poly (methyl methacrylate) blends, Express Polymer Letters, 1 (2007) 334-344.